

Formation and properties of mesoporous MoS₂ films

© A.B. Loginov¹, S.N. Bokova-Sirosh^{2,3}, P.V. Fedotov^{2,3}, I.V. Sapkov¹, D.N. Chmelenin⁴,
R.R. Ismagilov¹, E.D. Obratsova^{2,3}, B.A. Loginov⁵, A.N. Obratsov¹

¹ Department of Physics, Moscow State University,
119991 Moscow, Russia

² Prokhorov Institute of General Physics, Russian Academy of Sciences,
119991 Moscow, Russia

³ Moscow Institute of Physics and Technology (National Research University),
141701 Moscow Oblast, Dolgoprudny, Russia

⁴ Federal Scientific Research Center „Crystallography and Photonics“, Russian Academy of Sciences,
119333 Moscow, Russia

⁵ National Research University of Electronic Technology,
124498 Moscow, Russia

E-mail: loginov.ab15@physics.msu.ru

Received September 23, 2022

Revised November 14, 2022

Accepted December 9, 2022

Molybdenum disulfide is a crystalline material which attracts considerable attention due to explicit two-dimensional character of its electronic properties. To obtain MoS₂ films thermally evaporated molybdenum and gaseous H₂S were used as precursors in this work. As a result of chemical reaction of these precursors films consisting of flake-like of nanometer thickness assembled from parallel atomic layers with predominantly perpendicular (with respect to substrate surface) orientation were deposited on the surface of Si substrate. In this work we investigate the dependence of film morphology on deposition time, substrate temperature and concentration of precursors in gaseous phase. Presence of mono- and bi-layered structures in the film was revealed using Raman spectroscopy and electron microscopy. Dependence of photoluminescence properties on size of crystallites in produced films was also studied.

Keywords: 2D materials, transition metal dichalcogenides, flakes, monolayers, mesoporous films.

DOI: 10.21883/SC.2022.12.55146.4129

1. Introduction

The interest in fabrication, examination, and application of materials with a two-dimensional nature of their physical properties has been on the rise lately [1,2]. The pioneering studies of K. Novoselov and A. Geim into the electronic properties of graphene [3] stimulated numerous researches in this area. Two-dimensional properties of graphene are manifested in record-high values of specific conductivity and carrier mobility and in the capacity to absorb light within a wide wavelength interval (including, among others, ultraviolet, visible, and near and far infrared ranges). A zero bandgap of an ideally flat graphene makes it especially well-suited for high-frequency (up to the terahertz range) applications [4]. Other two-dimensional materials, such as hexagonal boron nitride, two-dimensional black phosphorus, and the whole class of materials known as transition-metal dichalcogenides (TMDs) [5], can be viable alternatives to graphene. These and other two-dimensional materials and their combinations attract considerable attention both in fundamental research and in applied studies aimed at designing various electronic and photonic instruments and devices.

Specifically, TMDs have similar crystal structures, and their general chemical formula is MX₂, where M is a transition metal (Mo, W, Ta, V, Nb, etc.) and X is a chalcogen

(S, Se, Te). The electronic properties of TMDs vary within a wide range: they may act like metals, dielectrics, or semiconductors with different bandgaps. This variability of characteristics of different transition metals, which have approximately the same crystal structure, is attributed to different amount of *d* electrons of different transition metal atoms. These electrons do not form chemical bonds, but contribute to band filling [6]. Monolayers of semiconductor TMDs are particularly well-suited for optoelectronics, since these materials transform into direct-gap ones when the number of layers reaches its minimum, and the rates of electronic transitions with photon absorption or emission increase several-fold [7]. The large mass of lattice atoms and the lack of an inversion center in TMDs also make effects related to the spin-orbit interaction especially well-pronounced. This opens the way for their application in advanced spintronic and valleytronic devices [8,9].

Similarly to graphene TMDs can be obtained by mechanical exfoliation of bulk crystals with a scotch-tape technique as one of the simplest and most widespread production methods [10]. Samples obtained this way are noted for their high purity and structural perfection; however, the size of their single-crystalline regions is limited to several tens of micrometers. In addition, the discussed method is suitable for production of individual TMD film samples only and is thus applicable solely in fundamental research.

Other methods actively being searched for at present, need to be developed to achieve reproducibility and scalability of production of such materials.

Chemical vapor deposition (CVD) has become one of the most widely used techniques for production of films of TMDs and other materials [11–13]. Its wide appeal is attributable in part to the relative simplicity of engineering implementation. A film material is formed in a CVD process as a result of chemical reactions between precursor molecules adsorbed from a gas medium onto the surface of a heated substrate. Under certain conditions, precursor molecules react with each other and the substrate in such a way that the reaction products crystallize and form a film on the substrate surface. The parameters of CVD synthesis of films with specific physical, structural, and morphological properties are commonly determined empirically (starting from fairly general preliminary assumptions).

Research efforts in TMD production are currently concentrated on the synthesis of films consisting of monolayer (as well as few- and multilayer) crystallites with atomic layers being parallel to the substrate. These „planar“ films are, with few exceptions [14], arrays of crystallites of a regular triangular shape with a nanometer thickness and longitudinal dimensions (length and width) up to several tens of micrometers that are arranged chaotically and oriented along the substrate surface. To examine the properties of such films and (or) fabricate certain devices based on them, one needs to localize single-crystalline regions and form the needed contact pads on them. This has a marked negative effect on the reproducibility of results and the scalability of processes [1].

One of the approaches providing a partial solution to this problem involves the fabrication of films consisting of flake-like crystallites with atomic layers oriented perpendicularly to the substrate surface. With the thickness of such crystallites decreased to nanometer range, the properties of such films may be similar to those of the corresponding mono-, few-, and multilayer structures. Notably, films of this morphology feature higher values of the specific surface area and the material volume per unit substrate area than films consisting of lateral crystallites. An example of materials of this kind is provided by mesoporous films of a similar morphology consisting of vertically aligned graphite crystallites of a nanometer thickness (also referred to as nanographite scales, flakes, nanowalls, etc.) that exhibit the properties typical of graphene [15]. Similar mesoporous TMD (e.g., MoS₂) films have been examined earlier as high-porosity catalyst carriers and materials for supercapacitors [16–18].

Precursors in powdered form, which are decomposed into constituent atoms and molecules under heating, are commonly used in the process of CVD synthesis of TMD films. The obtained gaseous precursors form a crystalline material on the substrate surface as a result of chemical reactions. In the present study, we used hydrogen sulfide gas, which flowed through an array of molybdenum filaments heated by an electric current to a temperature of metal

evaporation ($\sim 1500^\circ\text{C}$), to produce uniform film coatings consisting of vertically aligned flake-like MoS₂ crystallites of a nanometer thickness. This technical implementation allows one to speed up the fabrication of MoS₂ film coatings and achieve fine reproducibility, uniformity, and (potentially) scalability of the process. The structural and morphological properties and the composition of obtained film materials were analyzed by scanning and transmission electron microscopy (SEM and TEM), Raman spectroscopy, and photoluminescence (PL) spectroscopy (including photoluminescence excitation spectroscopy).

2. Experimental part

The diagram of the experimental setup for CVD synthesis of films consisting of vertically aligned MoS₂ flakes of a nanometer thickness is presented in Fig. 1. Hydrogen sulfide is introduced into a sealed chamber with a volume of 5 L (evacuated in advance to a pressure of 10^{-3} mbar using a rotary-vane forevacuum pump) via a quartz tube. The gas flow is controlled with a needle inlet valve. Adjusting the gas evacuation and inflow rates, we could maintain a steady pressure at the chosen level in the chamber. The flow of hydrogen sulfide is routed by the quartz tube to a system of molybdenum filaments with a thickness of $60\ \mu\text{m}$ that are positioned parallel to each other with a spacing of 1 mm. These filaments are heated by an electric current passing through them. Ohmic heat released in current passage was also used to heat the substrate that was made of standard polished single-crystalline silicon with a 300-nm-thick SiO₂ layer. The size of silicon substrates was $10 \times 5 \times 0.4$ mm. The substrate holder design, which provided a fairly low level of heat conduction, was detailed in [19].

The flow of hydrogen sulfide was adjusted with the needle inlet valve so that its pressure in the chamber was $7.5 \cdot 10^{-1}$ mbar in all experiments. A current of 0.77 A was passed through each molybdenum filament in all the

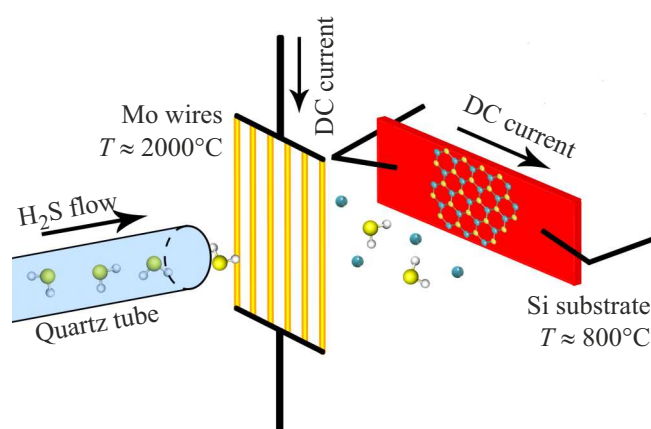


Figure 1. Diagram of the setup for CVD synthesis of films of vertically aligned MoS₂ flakes of a nanometer thickness: hydrogen sulfide from a quartz tube flows past heated molybdenum filaments and is directed to a substrate.

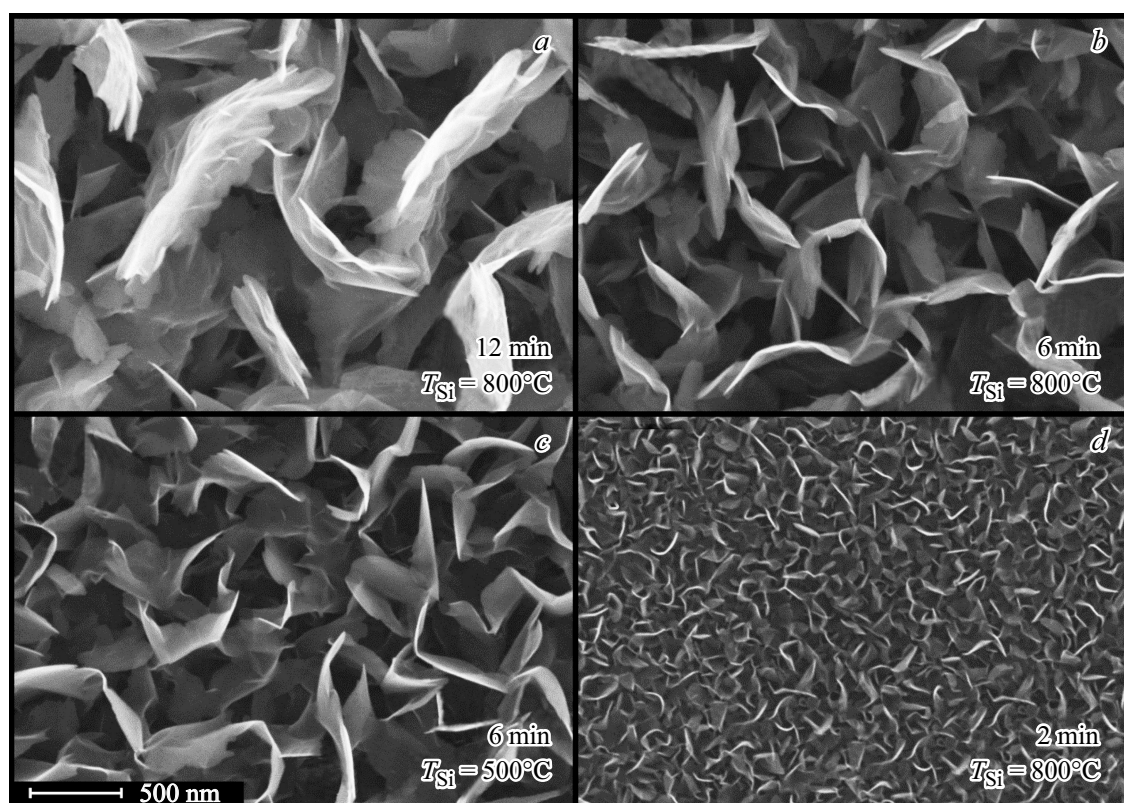


Figure 2. SEM images of MoS₂ films with a flake morphology. The scale is the same for all images. The silicon substrate temperature set in CVD synthesis and the film deposition time are indicated in each image. SEM images were obtained with an energy of the incident electron beam of 10 keV, a working distance of 10 mm, an aperture of 30 μm , and an incident beam current of ~ 300 pA.

synthesis processes discussed below. Their temperature increased to 1400°C as a result. The substrate temperature varied within the range of 500–800°C from one experiment to the other. The deposition time of different samples was also varied from 1 to 15 min.

The obtained film samples were examined with a Supra 40 (Carl Zeiss) scanning electron microscope, a HORIBA LabRAM HR Evolution UV–VIS–NIR–Open Raman spectrometer fitted with a confocal optical microscope (an Nd:YAG laser with $\lambda_{\text{ex}} = 532$ nm and a power of 14 mW was used for excitation), a FEI Tecnai Osiris transmission electron microscope, and a Horiba Jobin-Yvon NanoLog-4 PL spectrometer operating in the 180–850 nm range and fitted with an R928P photomultiplier. Photoluminescence was excited by a source (a Xe lamp and a double monochromator) integrated into the spectrometer.

3. Results and discussion

The synthesis parameters under which a film of vertically aligned nanowalls (flakes) forms on the substrate surface were determined in the course of preliminary studies. It was found that the longitudinal dimensions (length and height) of these flakes varied from several tens of nanometers to several micrometers depending on the synthesis parameters and

the deposition time. The transverse (thickness) dimensions of flakes did not exceed several nanometers. Typical SEM images of such films are presented in Fig. 2. For example, under otherwise equal process conditions, flakes grew in size from 100 nm at a deposition time of 2 min to 1 μm at 12 min. Smaller secondary flake-like structures were observed on flakes 1 μm in size. The flake size was found to be almost independent of the substrate temperature, which varied within the range of 500–800°C. At the same time, the growth rate (and, consequently, the size) of flakes depended on the pressure in the chamber. This is likely attributable to the expected variation of concentration of gaseous precursors. However, this dependence was not investigated systematically in the present study and is not discussed below (with the exception of effects related to the thermal evaporation of molybdenum filaments).

It was found that the film formation rate increased considerably when molybdenum filaments preannealed in vacuum were used in the deposition process. The process duration was 7–8 min for a film of flakes 100 nm in size formed using non-annealed molybdenum wires with a relatively smooth surface. If molybdenum filaments were preannealed in vacuum (10^{-3} mbar) at a temperature of $\sim 1500^\circ\text{C}$ for 7 min, the synthesis of the same film was completed in 1–2 min. This marked difference between deposition rates is likely attributed to the molybdenum

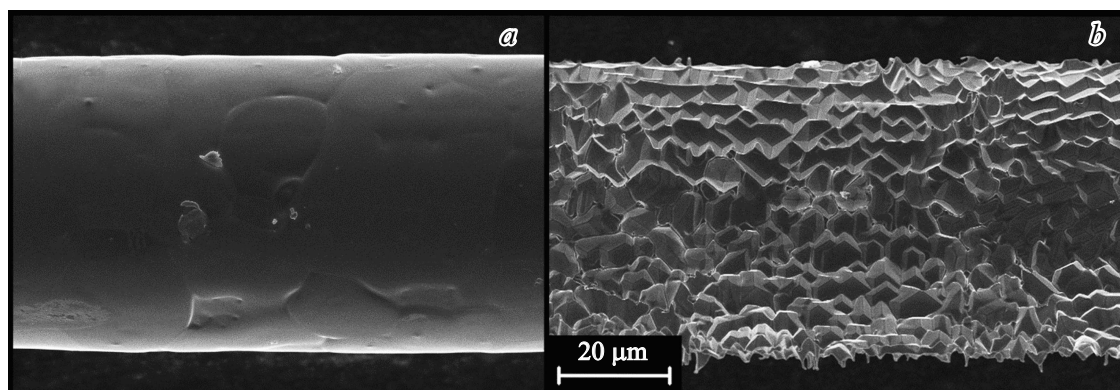


Figure 3. SEM images of the initial (non-annealed) molybdenum filament (*a*) and the filament subjected to annealing in vacuum (10^{-3} mbar) at a temperature of 1500°C for 7 min (*b*). The scale is the same for all images.

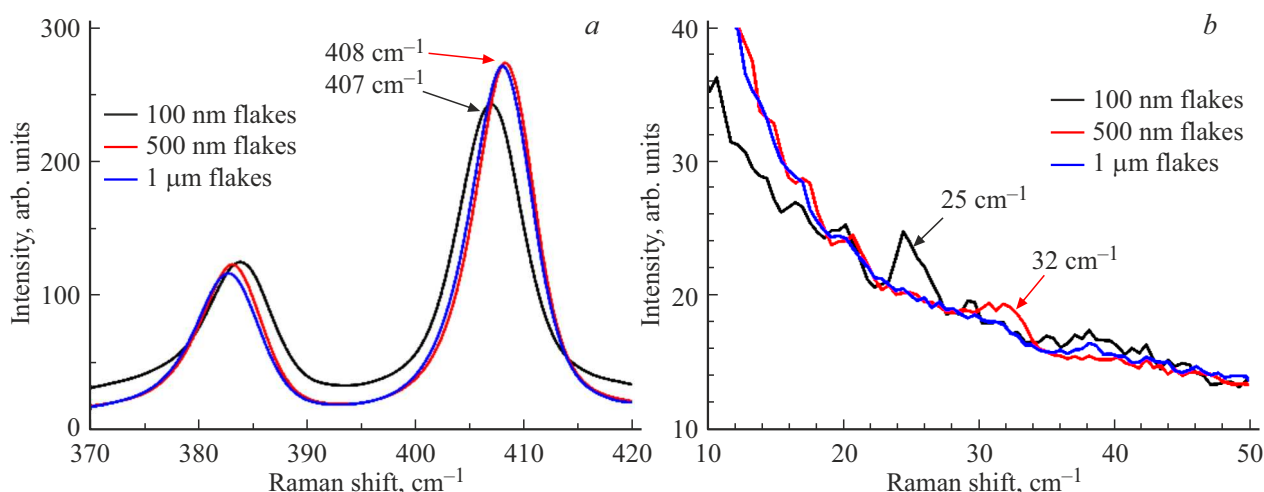


Figure 4. Raman spectra of MoS_2 films with a flake morphology: *a* — $370\text{--}420\text{ cm}^{-1}$ range, *b* — ultralow frequency range ($10\text{--}50\text{ cm}^{-1}$). (A color version of the figure is provided in the online version of the paper).

recrystallization in the process of preparatory annealing [20], thus transforming the initially smooth filament surface into a rough one. The resulting increase in the surface area of filaments translates into an enhanced efficiency of thermal evaporation of molybdenum and an increase in its concentration in the gas mixture. The results of SEM studies confirm that the surface of molybdenum filaments is modified in vacuum annealing (see Fig. 3). According to our estimates based on SEM images, the surface area of filaments increased by a factor of 15–20 after annealing. It should be noted that the surface of molybdenum filaments also undergoes a similar modification in the CVD process. Therefore, the effect of enhancement of the film deposition rate due to the use of molybdenum filaments preannealed in vacuum is manifested within the first 10 min of synthesis, but vanishes almost completely afterwards.

The examination of Raman spectra provided data characterizing the composition and the crystalline structure of the obtained film material. Figure 4, *a* shows the spectra of synthesized films featuring lines at 384 and 407 cm^{-1}

that are typical of crystalline MoS_2 . These lines shifted closer to each other as the size of flakes in films decreased. This pattern of behavior of spectra corresponded to a reduction in the number of layers in MoS_2 crystallites, which correlates with the flake size reduction [21]. Examining the Raman spectra in the low-frequency region, one may determine more accurately the number of atomic layers in MoS_2 flakes (see Fig. 4, *b*). Specifically, the line at 25 cm^{-1} , which is observed in crystallites 100 nm in size, corresponds to 2–3 layers of MoS_2 of polytype $2H$, while the spectra of films with flakes 500 nm in size feature a line at 32 cm^{-1} that corresponds to 5–6 layers of MoS_2 of polytype $2H$ [22,23]. These low-frequency lines were not found in the spectra of films with flakes $\sim 1\text{ }\mu\text{m}$ in size. This implies that MoS_2 structures of polytype $3R$ with more than 13 layers are dominant in them [23].

Both Raman and PL spectra (see below) were measured at room temperature. An Olympus LMPLFN $\times 50$ long-focus lens was used to focus excitation laser radiation to a spot with an approximate size of $1\text{ }\mu\text{m}$ on the substrate

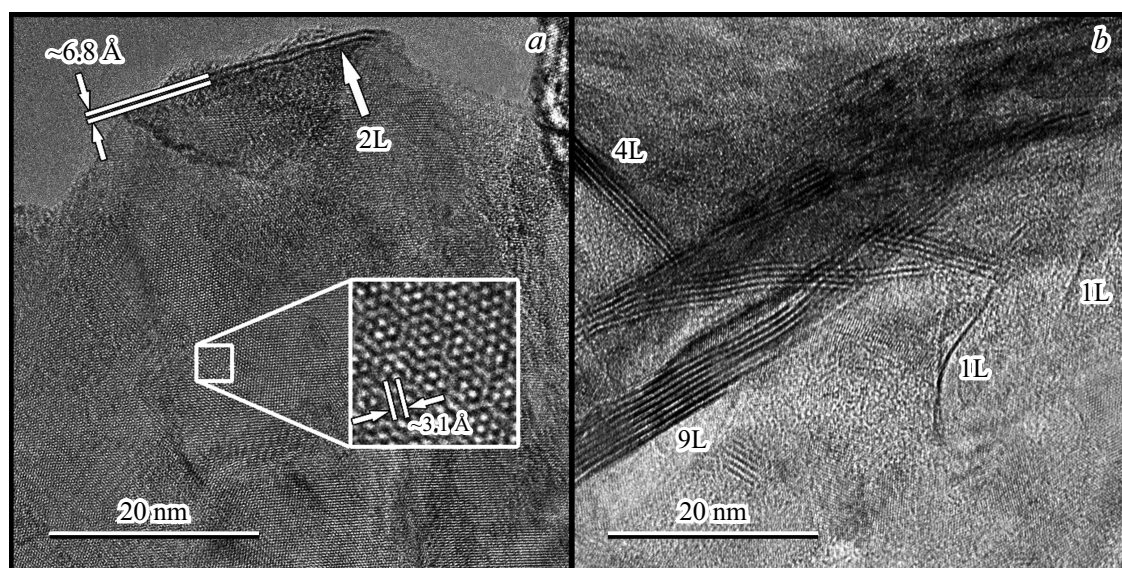


Figure 5. TEM images of a horizontal MoS₂ film part (*a*) and a film part with vertical structures (*b*). The number of layers in the structure is indicated next to it (1L, 2L, 4L, 9L). TEM images were obtained at an accelerating voltage of 200 kV and a beam current of ~ 1 nA.

surface. The excitation and measurements of Raman and PL signals were performed in the confocal arrangement with the microoptic spectrometer attachment.

High-resolution TEM studies were carried out to examine the structure of films in more detail. Samples for these studies were fabricated by introducing a film on its silicon substrate into fluoric acid (HF) to dissolve the intermediate layer of silicon oxide (SiO₂) with a thickness of 300 nm. Fragments of a film thus separated from the substrate were transferred to a copper mesh holder and subjected to TEM examination. The obtained results are presented in Fig. 5. A part immediately adjacent to the substrate could be identified in the studied fragments of films. The edges of this part of the film folded at certain sites in the region of fracture induced by the procedure of film transfer to the mesh holder, thus providing an opportunity to determine the number of atomic layers. Specifically, it was found that film parts immediately adjacent to the substrate consist of two MoS₂ layers (see Fig. 5, *a*). The interlayer distance is 6.8 ± 0.5 Å and agrees, within the margin of error, with literature data for monocrystalline MoS₂ [7,10,11]. The lattice symmetry and the characteristic lattice period (3.1 ± 0.2 Å) identified by examining the images of the atomic structure of this film part (see Fig. 5, *a*) also correspond to the structure of MoS₂.

Other fragments of films studied by TEM correspond to flake-like crystallites oriented perpendicularly to the substrate. The TEM image presented in Fig. 5, *b* is typical of these regions. Individual atomic layers are seen clearly in this image, and their number is easy to determine. Vertically aligned MoS₂ structures (nanowalls, flakes) typically consist of 8–10 layers. However, crystallites with a thickness of 4–5 layers and multilayer structures are also observed. The

observation of structures several monolayer in thickness agrees with the presence of low-frequency lines in Raman spectra (see Fig. 4, *b*).

The obtained film samples were also studied using PL spectroscopy. Figure 6, *a* presents the PL spectra of MoS₂ films with a flake morphology measured using the Raman spectrometer under excitation by laser radiation at a wavelength of 532 nm and normalized to the intensity of the 408 cm^{-1} Raman line. The examined PL spectra of films feature one well-pronounced peak at a wavelength of ~ 650 nm (corresponding to a photon energy of 1.9 eV). This agrees well with the data of earlier studies; the observed peak may be associated with the recombination of an *A* exciton at the *K/K'* point of the Brillouin zone, where direct electronic transitions are allowed [24–26].

It is fair to assume that the intensity of the primary Raman line at 408 cm^{-1} for uniform films is governed by their thickness and depends only weakly on the number of atomic layers in MoS₂ crystallites. The PL intensity, on the other hand, has a complex dependence on the number of layers. In order to factor in the influence of the number of layers, we normalized PL spectra to the intensity of the 408 cm^{-1} Raman line prior to comparing them. The spectra in Fig. 6, *a* indicate that the normalized PL intensity for films consisting of flakes ~ 100 nm in size is almost an order of magnitude higher than the one for films consisting of flakes with a size of ~ 0.5 – $1\ \mu\text{m}$. The ratio of intensities of PL (in the region of 650–665 nm) and Raman (408 cm^{-1}) lines is 1.8 for films consisting of flakes 100 nm in size, 0.2 for films with a characteristic flake size of 500 nm, and 0.09 in the case of flakes $\sim 1\ \mu\text{m}$ in size. A PL intensity similar to the one of films consisting of 100-nm-sized flakes was observed in MoS₂ monolayers on the SiO₂/Si substrate surface [27]. The

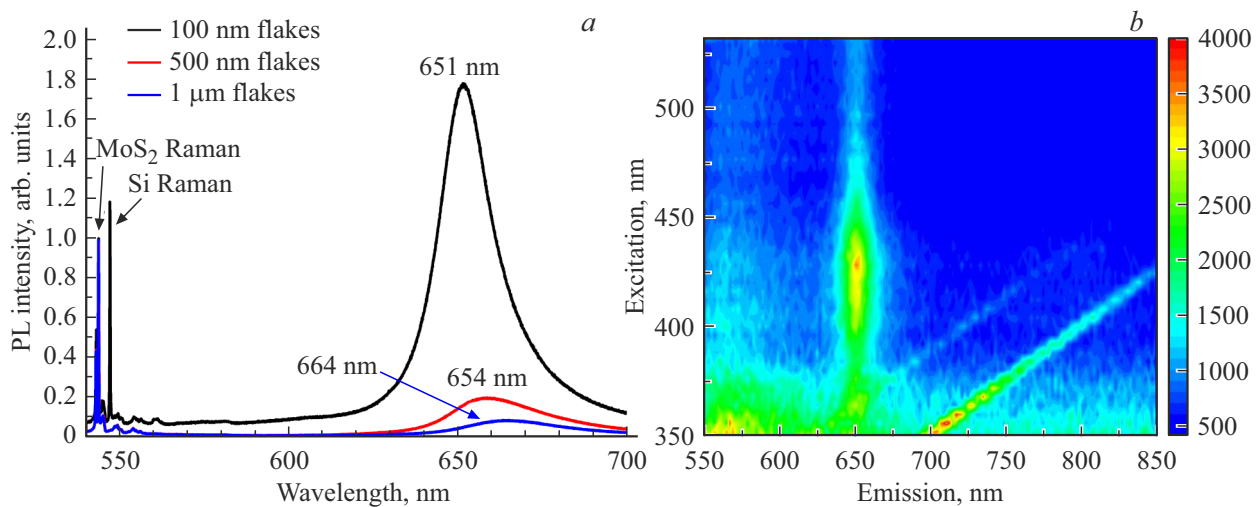


Figure 6. *a* — PL spectra normalized to the intensity of the Raman line at 408 cm^{-1} ; *b* — diagram of dependence of the PL intensity on the excitation wavelength for a MoS_2 film with a characteristic flake size of 100 nm. Inclined lines in panel *b* are artifacts induced by the measurement equipment.

observed high PL/Raman (408 cm^{-1}) intensity ratios are likely attributable, among other factors, to the fact that few- and monolayer structures, which were identified by TEM and Raman spectroscopy (see above), have a significant presence in the composition of films. It should also be noted that the PL maximum undergoes a redshift when the flake size increases. This may be associated with the presence of internal stresses [28].

Parallel to examining the characteristics of photoluminescence under excitation by laser radiation with a wavelength of 532 nm, we studied the PL excitation spectra using a xenon lamp and a double monochromator that isolated the needed spectral emission interval. Figure 6, *b* presents a map characterizing the dependence of the PL intensity in different regions of the spectrum on the excitation wavelength. The dependence of intensity of the primary PL line ($\sim 650\text{ nm}$) is maximized under excitation at a wavelength of $\sim 425\text{ nm}$. In addition to the primary line ($\sim 650\text{ nm}$), relatively weak PL, which intensified under excitation by radiation with a wavelength falling within the 350–375 nm interval, was observed at shorter wavelengths (550–630 nm). The energy difference between the maxima of short-wave (550–570 nm) and primary (650 nm) PL components is 0.28–0.35 eV. Notably, the binding energy of an A exciton in MoS_2 was estimated at 0.22–0.57 eV in different studies [29–31]. This provides evidence in favor of the assumption that the long-wave PL component is associated with direct single-particle interband transitions near the K/K' point of the Brillouin zone. At the same time, it is known from literature that MoS_2 absorption spectra feature an additional resonance at a wavelength of $\sim 590\text{ nm}$ related to the production of a B exciton [25]. The short-wave PL line may be attributed to the process of radiative recombination of a B exciton. A thorough analysis of the origin of this short-wave PL and its dependence on the

excitation radiation wavelength will be performed in future studies.

4. Conclusion

A novel variation of the method of CVD synthesis of MoS_2 films from gaseous precursors (molybdenum vapor and hydrogen sulfide) was developed in the present study. The substrate for MoS_2 deposition was made of silicon with a 300-nm-thick SiO_2 oxide layer. Molybdenum vapor was produced via thermal evaporation of filaments. Hydrogen sulfide flowed past heated molybdenum filaments and transferred metal vapor to the substrate surface. The obtained films were aggregates of flake-like MoS_2 crystallites of a nanometer thickness with a preferred orientation along the normal to the substrate surface. The longitudinal dimensions of crystallites (length and height) varied from 100 nm to 0.5–1 μm depending on the deposition time and other process parameters. Compared to the known methods, the developed synthesis technique provides an opportunity to enhance considerably the rate of MoS_2 film deposition.

Films with longitudinal flake dimensions of $\sim 100\text{ nm}$ synthesized within 1–2 min contain a significant amount of monolayer MoS_2 fragments.

Funding

The work on formulating the problem, drafting the research plan, and synthesizing film materials was performed under state assignment „Crystallization Physics and Properties of Crystals and Films“ (state registration No. 01200803994). The study of morphological properties of films was supported by grant No. 21-2-10-34-1 from Theoretical Physics and Mathematics Advancement Foundation „BAZIS“. Optical research was performed with

support from the Russian Science Foundation (grant No. 20-42-08004). Equipment provided by the common use center of FSRC „Crystallography and Photonics“, Russian Academy of Sciences, was used to carry out structural studies by transmission electron microscopy. These studies were supported financially by the Ministry of Science and Higher Education of the Russian Federation under the state assignment of FSRC „Crystallography and Photonics“.

Conflict of interest

The authors declare that they have no conflict of interest.

References

- [1] Y. Sheng, T. Chen, Y. Lu, R.-J. Chang, S. Sinha, J. H. Warner. *ACS Nano*, **13** (4), 4530 (2019).
- [2] J. Yao, G. Yang. *Small*, **14** (21), 1704524 (2018).
- [3] A.K. Geim, K.S. Novoselov. *Nature Materials*, **6**, 183 (2007)
- [4] F. Schwierz. *Nature Nanotechnol.*, **5** (7), 487 (2010).
- [5] G.R. Bhimanapati, Z. Lin, V. Meunier, Y. Jung, J. Cha, S. Das, D. Xiao, Y. Son, M.S. Strano, V.R. Cooper, L. Liang, S.G. Louie, E. Ringe, W. Zhou, S.S. Kim, R.R. Naik, B.G. Sumpter, H. Terrones, F. Xia, Y. Wang, J. Zhu, D. Akinwande, N. Alem, J.A. Schuller, R.E. Schaak, M. Terrones, J.A. Robinson. *ACS Nano*, **9** (12), 11509 (2015).
- [6] S. Manzeli, D. Ovchinnikov, D. Pasquier, O.V. Yazyev, A. Kis. *Nature Rev. Mater.*, **2**, 17033 (2017).
- [7] K.F. Mak, J. Shan. *Nature Photonics*, **10** (4), 216 (2016).
- [8] Y.P. Feng, L. Shen, M. Yang, A. Wang, M. Zeng, Q. Wu, S. Chintalapati, C.-R. Chang. *WIREs Comput. Mol. Sci.*, **7** (5) (2017).
- [9] J.R. Schaibley, H. Yu, G. Clark, P. Rivera, J.S. Ross, K.L. Seyler, W. Yao, X. Xu. *Nature Rev. Mater.*, **1** (11), 16055 (2016).
- [10] B.W.H. Baugher, H.O.H. Churchill, Y. Yang, P. Jarillo-Herrero. *Nano Lett.*, **13** (9), 4212 (2013).
- [11] V.K. Kumar, S. Dhar, T.H. Choudhury, S.A. Shivashankar, S. Raghavan. *Nanoscale*, **7** (17), 7802 (2015).
- [12] V.O. Borisov, R.R. Ismagilov, A.A. Zolotukhin, A.N. Obraztsov. *J. Nanoelectron. Optoelectron.*, **8** (1), 100 (2013).
- [13] A.B. Loginov, I.V. Bozhev, S.N. Bokova-Sirosh, E.D. Obraztsova, R.R. Ismagilov, B.A. Loginov, A.N. Obraztsov. *Appl. Surf. Sci.*, **494**, 1030 (2019).
- [14] Y. Yu, C. Li, Y. Liu, L. Su, Y. Zhang, L. Cao. *Sci. Rep.*, **3** (1), 1866 (2013).
- [15] R.G. Zonov, G.M. Mikheev, A.N. Obraztsov, Yu.P. Svirko. *Opt. Lett.*, **45** (7), 2022 (2020).
- [16] M.H. Johari, M.S. Sirat, M.A. Mohamed, S.N.F. Mohd Nasir, M.A. Mat Teridi, A.R. Mohamad. *Nanotechnology*, **31** (30), 305710 (2020).
- [17] J. Xie, H. Qu, J. Xin, X. Zhang, G. Cui, X. Zhang, J. Bao, B. Tang, Yi Xie. *Nano Res.*, **10** (4), 1178 (2017).
- [18] J. Xie, H. Qu, J. Xin, X. Zhang, G. Cui, X. Zhang, J. Bao, B. Tang, Y. Xie. *Nano Res.*, **10** (4), 1178 (2017).
- [19] A.B. Loginov, I.V. Bozhev, S.N. Bokova-Sirosh, E.D. Obraztsova, R.R. Ismagilov, B.A. Loginov, A.N. Obraztsov. *Tech. Phys.*, **64** (11), 1666 (2019).
- [20] S. Primig, H. Leitner, H. Clemens, A. Lorich, W. Knabl, R. Stickler. *Int. J. Refract. Met. Hard Mater.*, **28** (6), 703 (2010).
- [21] H. Li, Q. Zhang, C.C.R. Yap, B. Kang Tay, T.H.T. Edwin, A. Olivier, D. Baillargeat. *Adv. Funct. Mater.*, **22** (7), 1385 (2012).
- [22] R.T. Sam, T. Umakoshi, P. Verma. *Sci. Rep.*, **10** (1), 21227 (2020).
- [23] J. van Baren, G. Ye, J.-A. Yan, Z. Ye, P. Rezaie, P. Yu, Z. Liu, R. He, C.H. Lui. *2D Mater.*, **6** (2), 025022 (2019).
- [24] R. Coehoorn, C. Haas, R.A. de Groot. *Phys. Rev. B*, **35** (12), 6203 (1987).
- [25] K.F. Mak, C. Lee, J. Hone, J. Shan, T.F. Heinz. *Phys. Rev. Lett.*, **105** (13), 136805 (2010).
- [26] A. Steinhoff, J.-H. Kim, F. Jahnke, M. Rösner, D.-S. Kim, C. Lee, G.H. Han, M.S. Jeong, T.O. Wehling, C. Gies. *Nano Lett.*, **15** (10), 6841 (2015).
- [27] A. Splendiani, L. Sun, Y. Zhang, T. Li, J. Kim, C.-Y. Chim, G. Galli, F. Wang. *Nano Lett.*, **10** (4), 1271 (2010).
- [28] H.J. Conley, B. Wang, J.I. Ziegler, R.F. Haglund, S.T. Pantelides, K.I. Bolotin. *Nano Lett.*, **13** (8), 3626 (2013).
- [29] N. Saigal, V. Sugunakar, S. Ghosh. *Appl. Phys. Lett.*, **108** (13), 132105 (2016).
- [30] C. Zhang, A. Johnson, C.-L. Hsu, L.-J. Li, C.-K. Shih. *Nano Lett.*, **14** (5), 2443 (2014).
- [31] A.R. Klots, A.K.M. Newaz, B. Wang, D. Prasai, H. Krzyzanowska, J. Lin, D. Caudel, N.J. Ghimire, J. Yan, B.L. Ivanov, K.A. Velizhanin, A. Burger, D.G. Mandrus, N.H. Tolk, S.T. Pantelides, K.I. Bolotin. *Sci. Rep.*, **4** (1), 6608 (2014).